Colloid Polym Sci 275:1010–1017 (1997)

ORIGINAL CONTRIBUTION

M. Ocaña
M. Martínez-Gallego

Preparation by hydrolysis of aerosols and properties of Cr, Mn and Co doped alumina spherical particles

Received: 15 April 1997
Accepted: 25 June 1997

Dr. M. Ocaña (✉)
Instituto de Ciencia de Materiales
de Sevilla (C.S.I.C.-UNSE)
Americo Vespucio s/n
Isla de La Cartuja
41092 Sevilla, Spain

M. Martínez-Gallego
Departamento de Química Inorgánica
Universidad de Extremadura
Avda. de Elvas s/n
Badajoz, Spain

Abstract A method for the preparation of chromium-doped (pink), manganese-doped (brown) and cobalt-doped (blue) alumina pigments consisting of spherical particles of broad size distribution (<5 μm) is reported. The procedure, based on the room-temperature hydrolysis of aerosols generated from a mixture of aluminum *sec*-butoxide and a solution of the corresponding metal nitrates in *sec*-butanol, yields amorphous solids. The temperature of calcination and the composition of the so produced powders were varied to investigate their effects on the color properties of the pigments, which were also characterized in terms of their composition, crystalline structure and electrokinetic behavior.

Key words Aerosols – spherical particles – Cr(III) doped alumina – Mn(II) doped alumina – Co(II) doped alumina – pigments

Introduction

Cr(III)-doped, Mn(II)-doped and Co(II)-doped alumina find important applications in the field of ceramic pigments [1]. Such materials are commercially prepared by the traditional method which involves milling of the starting mixture of components for homogenization, calcination of this mixture to develop the crystalline phases and colors and a final grinding process to reduce particle size, after which particles of irregular size and shape usually result. It is amply recognized that the availability of pigment particles with uniform shape and controlled size distribution would be highly desirable for a more precise control of their color properties.

In this paper, we describe the preparation of Cr(III)-doped, Mn(II)-doped and Co(II)-doped alumina powders through the hydrolysis of liquid aerosols [2, 3], which has been previously used to produce single- [4–7] and mixed-metal oxide powders [8, 9] and to incorporate organic compounds to inorganic matrices [10, 11]. This aerosol method always yields spherical particles since each droplet behaves as an independent reactor, whereas their size distribution can be controlled by adjusting the conditions of the aerosol generation (type of generator, gas flow rates, etc.). Therefore, the reproducibility of the color properties of the so prepared pigments is guaranteed. Two additional advantages of the reported procedure over the conventional one are its simplicity (grinding is eliminated) and continuous character which make it suitable for large-scale production.

As a rule, the method of hydrolysis of aerosols requires liquid precursors with a sufficiently high hydrolysis rate as to produce solid particles in a few seconds [12]. Such a requirement is fulfilled by aluminum *sec*-butoxide which was used as the starting precursor for alumina. Liquid and highly hydrolyzable compounds of the selected doping metals (Cr, Co, or Mn) were not available. However, the incorporation of these cations to the alumina matrix could be carried out by entrapping alcoholic solutions of the

CPS 878

corresponding metal nitrate in the solid particles during their formation process. The resulting amorphous powders were calcined to produce the desired crystalline phases and colors. The raw composition and the heating temperature were systematically varied to evaluate their effects on the color properties of the pigments, which were also characterized in terms of their particle size and shape, crystalline structure, composition, and electrokinetic behavior.

Experimental

Powder preparation

Aluminum *sec*-butoxide (Aldrich, 97%), $Cr(NO_3)_3 \cdot 9H_2O$ (Aldrich, 99%), $Co(NO_3)_2 \cdot 9H_2O$ (Aldrich, 99%) and $Mn(NO_3)_2 \cdot 6H_2O$ (Aldrich, 98%) were used as supplied.

The aerosols were generated by spraying a liquid mixture with the desired M/Al mole ratio (M = Cr, Mn or Co) prepared by mixing, under magnetic stirring, equal volumes of the aluminum alkoxide and a solution in *sec*-butanol of the corresponding metal salt. Nitrogen at constant pressure (0.5 kp cm^{-2}) was used as a carrier gas. The aerosols were then hydrolyzed at room temperature with water vapors introduced into the reaction chamber by bubbling nitrogen (flow rate = 2 $dm^3 min^{-1}$) through a water container. The resulting solid particles were finally collected using nylon sieves. A schematic diagram of the apparatus used for the entire process can be found in ref. [13].

The as-prepared powders were calcined at constant temperature for 4 h using platinum crucibles.

Powders characterization and color measurements

The particle size and shape of the samples were examined by scanning electron microscopy (SEM, JEOL JSM5400). The size distribution was evaluated from the electron micrographs by counting several hundreds of particles.

The composition of the as-prepared powders was determined by plasma emission (ICP, Perkin-Elmer 5500), where the samples were dissolved in concentrated HCl and the solutions diluted in doubly distilled water before analyses. The composition of the Cr_2O_3–Al_2O_3 solid solutions generated in the heated samples was estimated from the unit cell parameters of the corundum phase by using Vegards's law. Unit cell parameters were determined from the X-ray diffraction data collected in a Siemens D501 difractometer, using Cu K_α radiation, between 10–120° (2θ) at intervals of 0.04° (2θ) and for an accumulation time interval of 20 s. The powdered samples were mechanically mixed with a silicon standard (20% by weight). The crystallographic data for α-alumina and silicon were taken from refs. [14, 15], respectively. X-ray diffraction was also used to identify the different phases present in the solids.

To record the infrared spectra (Nicolet 20SXC), the powders were diluted in KBr. Differential thermal (DTA) and thermogravimetric (TGA) analyses (STA 781) were carried out in air at a heating rate of 10 °C min^{-1}.

The isoelectric point (i.e.p.) of the samples were determined (Coulter Delsa 440) by measuring electrophoretic mobilities of aqueous dispersions as a function of pH. For this, 15 mg of sample were dispersed in 100 cm^3 of a 0.01 mol dm^{-3} NaCl solution to keep the ionic strength constant while the pH was varied by adding HCl or NaOH as needed.

The color of the pigments was evaluated according to the CIE$L^*a^*b^*$ system [16]. In this color space, L^* is the color lightness ($L^* = 0$ for black and $L^* = 1$ for white), a^* is the green (−)–red (+) axis, and b^* is the blue (−)–yellow (+) axis. For this purpose, powdered layers containing a constant amount of sample (6 mg/cm^2) were prepared by filtering aqueous dispersions (40 mg of sample in 50 cm^3 of doubly distilled water) through Millipore membranes (pore size = 0.22 μm). The $L^*a^*b^*$ parameters of these pigment layers deposited on the membranes were then measured for a light source C, with a Dr. Lange LUCI 100 colorimeter, using a white tile (chromaticity coordinates, $x = 0.315$ and $y = 0.335$) as standard reference.

Results and discussion

Cr-doped alumina

In order to investigate the influence of the powders composition on their color properties, we prepared samples with different Cr/Al mole ratio (3%, 7% and 12%). The comparison between the nominal composition of these samples and that measured by ICP (Table 1) confirms the incorporation of Cr to the alumina matrix. It should be noted that the Cr concentration could not be increased above 12.5% (sample 12.5Cr) since in these conditions, the high amount of water associated to the chromium salt ($Cr(NO_3)_3 \cdot 9H_2O$), caused the instantaneous hydrolysis of the aluminum alkoxide during mixing.

All the Cr–Al_2O_3 samples prepared showed a similar thermal behavior. Most of the characterization data presented hereafter correspond to sample 12.5Cr (Table 1) chosen as a representative example. The as-prepared

Colloid & Polymer Science, Vol. 275, No. 11 (1997)

Table 1 Nominal and measured composition (M/Al mole ratio, with M = Cr, Mn or Co) for the M-doped alumina samples

Sample	M/Al mole ratio % Nominal	M/Al mole ratio % Measured
12.5Cr	12.0	12.5
8Cr	7.0	8.0
4Cr	3.0	4.0
10.8Mn	10.0	10.8
8.5Mn	8.0	8.5
6.1Mn	6.0	6.1
2.8Mn	2.5	2.8
10.7Co	10.0	10.7
5.3Co	5.0	5.3
2.8Co	2.5	2.8

particles were spherical, having diameters ranging from 0.2 to 5 μm (Fig. 1A). This broad size distribution gave a mean diameter (d_m) of 1.2 μm and a standard deviation (σ) of 0.8. X-ray diffraction showed that this powder was amorphous which is a general characteristic of powders produced by aerosol hydrolysis due to the low reaction temperature (room) and the high reaction rate [2]. The infrared spectrum of the sample (Fig. 2) displayed bands at 925 and 565 cm^{-1} mainly associated to Al–O vibrations [6] and at 1380 and 815 cm^{-1} due to the nitrate anions [17] coming from the chromium salt. Finally, absorptions at 3440 (not shown in the figure) and 1630 cm^{-1} were also observed which indicate the presence of a high amount of water in the sample.

Figure 3 shows the DTA curve obtained for sample 12.5Cr. The broad endothermic peak at about 100 °C is attributed to the release of adsorbed water, whereas the exothermic one at 185 °C could be due to the decomposition of residual organic species (*sec*-butanol and unreacted alkoxide groups). Two additional exothermic effects were detected at 325 °C and 860 °C, respectively. The first one is associated to the decomposition of the nitrate anions in agreement with the disappearance of the infrared nitrate bands (1380 and 815 cm^{-1}) after heating at 400 °C (Fig. 2). TGA analysis showed a weight loss (51%) between 25 °C and 500 °C, mainly due to the above processes. As a consequence, a shrinkage of the spherical particles (d_m = 0.8 μm and σ = 0.6) was detected (Fig. 1B). The exothermic peak at 860 °C was due to the crystallization of η-Al_2O_3, as will be substantiated later.

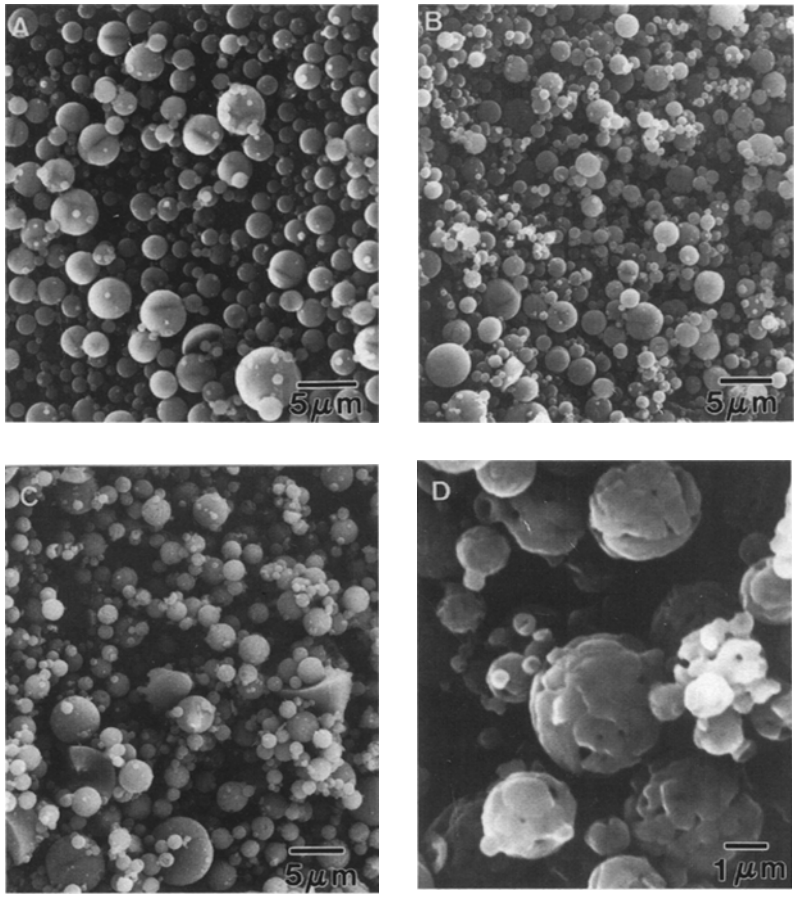

Fig. 1 SEM micrographs of sample 12.5Cr as prepared (A) and after heating at 500 °C (B), 1200 °C (C) and 1400 °C (D)

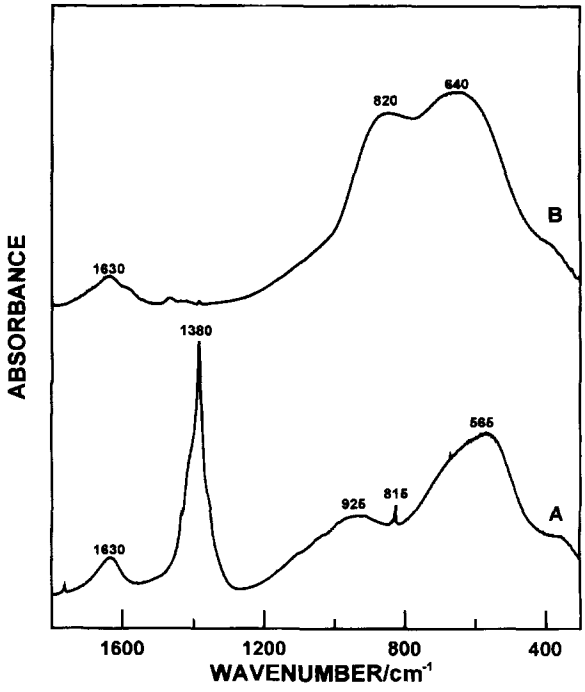

Fig. 2 Infrared spectra of sample 12.5Cr as prepared (A) and after heating at 400 °C (B)

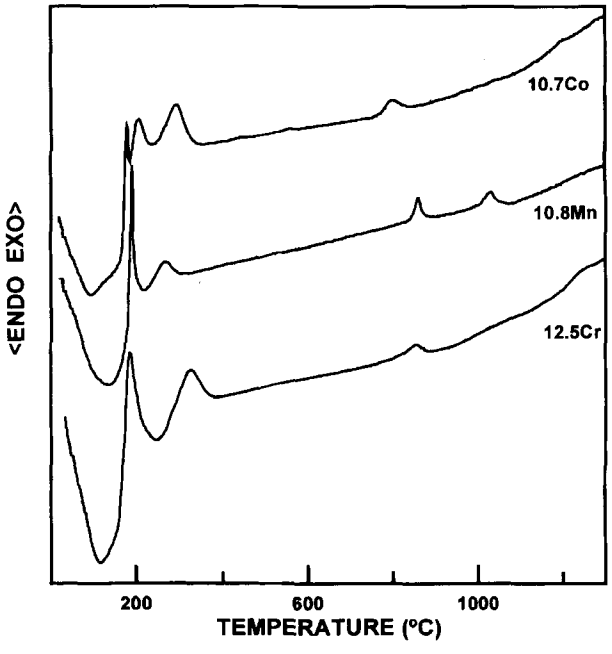

Fig. 3 Differential thermal analysis of samples 12.5Cr, 10.8Mn and 10.7Co

According to X-ray diffraction, sample 12.5Cr remained amorphous up to 600 °C. After heating at 700 °C, weak peaks due to Cr_2O_3 (corundum) were identified in the pattern (Fig. 4). Additional peaks were also observed

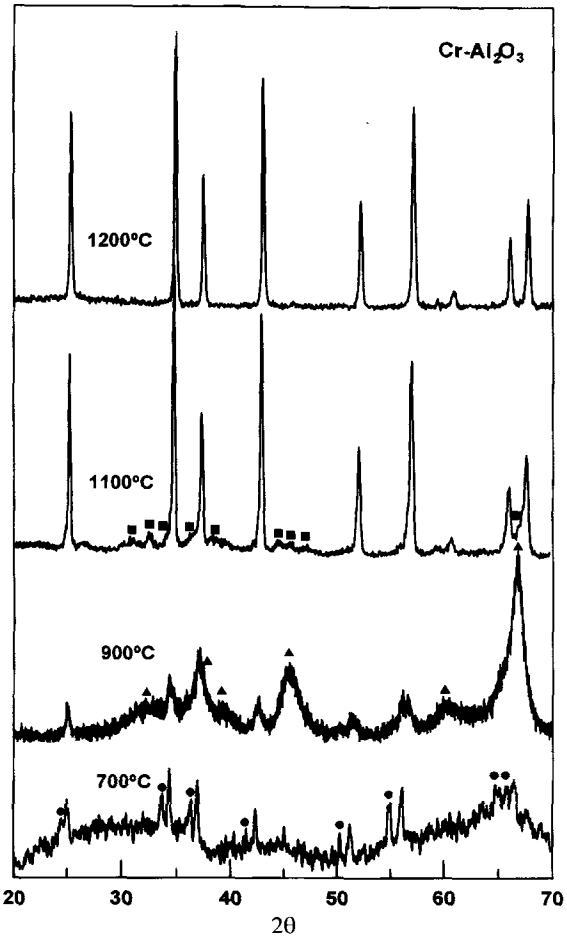

Fig. 4 X-ray diffraction patterns obtained for sample 12.5Cr after heating at different temperatures. Symbols designating different phases: (●) Cr_2O_3 (▲) η-Al_2O_3, (■) δ-Al_2O_3. Unlabelled peaks correspond to Cr_2O_3–Al_2O_3 solid solutions

at 2θ values intermediate between those corresponding to Cr_2O_3 and α-Al_2O_3, suggesting the formation of a Cr_2O_3–Al_2O_3 solid solution by incorporation of some Al^{3+} cations to the Cr_2O_3 lattice. The Cr/Al mole ratio determined for the latter by using Vegard's law was 62.5 ± 5% (Table 2). This value is approximated since the error in the estimation of cell parameters is rather high (Table 2) as a consequence of the low intensity of the peaks. The presence in the pattern of the heated sample of very broad features centered at 2θ—30°, 45° and 65° manifests that some material still remained amorphous in the sample, which crystallized into η-Al_2O_3 on calcination at 900 °C (Fig. 4), explaining the exothermic effect at 860 °C detected by DTA (Fig. 3). It should be noted that although the X-ray diffraction patterns of γ-Al_2O_3 and η-Al_2O_3 are very similar [18, 19], in this case, the crystalline phase comes from an amorphous material which is expected to

Colloid & Polymer Science, Vol. 275, No. 11 (1997)

Table 2 Unit cell *a* parameter and composition of the Cr_2O_3–Al_2O_3 solid solutions developed in sample 12.5Cr after calcination at different temperatures. Errors are given in parenthesis

Heating temperature [°C]	a [Å]	Cr/Al [%]
700	4.8831 (0.010)	62.5 (5.0)
900	4.8513 (0.007)	46.6 (3.5)
1100	4.7900 (0.001)	16.1 (0.5)
1200	4.7837 (0.001)	12.9 (0.5)

give only η-Al_2O_3 upon heat treatment [20]. This crystallization process was accompanied by the disappearance of the Cr_2O_3 peaks and the shift of those corresponding to the solid solution to higher 2θ values (Fig. 4). Such a behavior resulted in a decrease of the Cr/Al mole ratio to $46.6 \pm 3.5\%$ (Table 2) indicating a progress in the incorporation of Al^{3+} cations to the corundum lattice. This process proceeded on calcination at still higher temperatures. Thus, at 1100 °C a solid solution with a Cr/Al ratio of $16.1 \pm 0.5\%$ (Table 2) represented the major phase in the sample (Fig. 4). In fact, only a small amount of δ-Al_2O_3 was still present which completely disappeared at 1200 °C (Fig. 6). At this temperature, the Cr/Al mole ratio of the solid solution ($12.9 \pm 0.5\%$) (Table 2) was in agreement with that of the original sample (12.5%) (Table 1), suggesting the complete interdiffusion of the two corundum phases. It should be noted that after this heat treatment, the particles retained the spherical shape as observed in Fig. 1C which, after a careful examination, also shows their polycrystalline nature. No further structural changes were detected in sample 12.5Cr on heating at higher temperatures ($\leq$1400 °C). A certain particle sintering was only noticed when the sample was calcined at 1400 °C (Fig. 1D).

Cr-doped alumina is classified as a solid-solution pigment with corundum structure [11], which depending on the Cr content presents reddish (Cr/Al < 50%) or green (Cr/Al > 50%) colors [21]. Therefore, the color properties were only measured for samples heated at different temperatures above that corresponding to the complete formation of the Cr_2O_3–Al_2O_3 solid solution ($\geq$1200 °C). As observed in Table 3, the values of a^* and b^* for sample 12.5Cr heated at 1200 °C correspond to a lilac color. The temperature increase up to 1400 °C did not induce any noticeable change in color hue, in agreement with the absence of structural changes during treatment (Fig. 4). However, a slight decrease of luminosity (L^*) from 68.4 (1200 °C) to 64.0 (1400 °C) was observed, probably as a consequence of the increase of particle size resulting from the sintering process. The decrease in the Cr/Al mole ratio of the samples heated at 1200 °C to 8% (sample 8Cr, Table 1) gave rise to an increase of the a^* value and a decrease of the b^* value, involving a change of the color tint to pale pink. This change was accompanied by an increase of L^* (74.6) (Table 3), i.e., by a decrease of the color intensity. When the Cr/Al mole ratio was further decreased to 4% (sample 4Cr), a similar color hue (a^* and b^* parameters) was observed although with lower intensity (higher L^*) (Table 3).

Electrophoretic mobilities of sample 12.5Cr heated at 1200 °C are plotted as a function of pH in Fig. 5, along with those of a pure alumina sample, prepared by using a similar procedure (blank), which is included for comparison. As observed, the i.e.p. obtained for both samples was similar (5.2), being in the range reported [22] for α-Al_2O_3 (5–9.2). Therefore, it seems that the substitution of 12.5% of Al^{3+} cations by Cr^{3+} in the corundum lattice has no significant effect on the electrokinetic behavior of this material.

Table 3 C.I.E.$L^*a^*b^*$ parameters of the doped alumina samples heated at different temperatures

Sample	Temperature [°C]	L^*	a^*	b^*	Color
12.5Cr	1200	68.4	− 0.2	2.1	Lilac
12.5Cr	1400	64.0	0.9	1.2	Lilac
8Cr	1200	74.6	3.8	− 0.9	Pale pink
4Cr	1200	80.5	4.4	− 0.3	Pale pink
10.8Mn	1100	54.0	12.9	13.8	Strong brown
10.8Mn	1400	54.9	13.9	13.8	Strong brown
8.7Mn	1100	55.3	11.0	13.0	Strong brown
6Mn	1100	60.9	12.1	14.4	Strong brown
2.8Mn	1100	68.1	8.2	10.0	Light brown
10.7Co	1100	56.5	− 6.0	− 34.3	Blue
10.7Co	1300	55.3	− 6.4	− 34.9	Blue
5.3Co	1100	61.0	− 9.0	− 27.7	Blue
2.8Co	1100	64.7	− 6.0	− 26.5	Blue

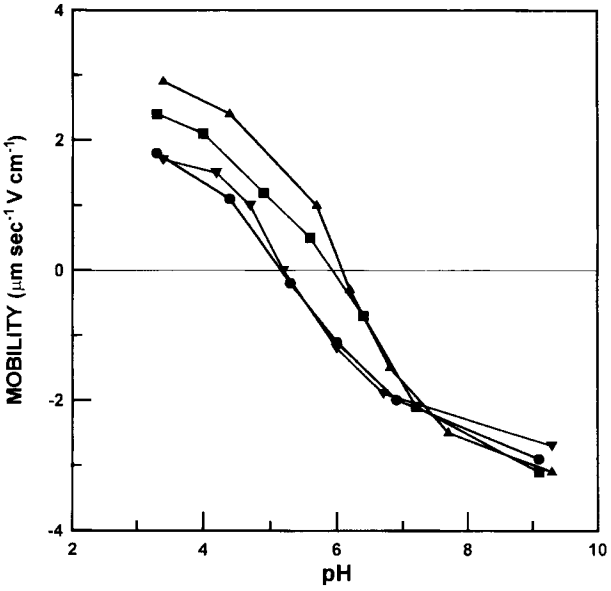

Fig. 5 Electrophoretic mobilities measured as a function of pH for samples 12.5Cr (●), 10.8Mn (▲), 10.7Co (■) and for an alumina blank (▼)

Mn-doped alumina

The rather good agreement between the nominal and measured compositions of the as-prepared Mn-doped alumina samples (Table 1) indicates the incorporation to the alumina matrix of the total amount of Mn(II) added to the aluminum alkoxide. As expected, these samples showed the same amorphous nature and morphological characteristics (particle size and shape) of the Cr-doped powders (Fig. 1A), since the experimental conditions used for the generation and hydrolysis of the aerosol were identical in both cases. The as-prepared Mn-doped samples also contained water and nitrate anions showing a thermal behavior at $<500\,^{\circ}C$ similar to that of Cr-doped samples (Fig. 3). However, some differences were noticed above this temperature. Thus, two exothermic effects were detected at 875 °C and 1050 °C, which, as indicated by X-ray diffraction, are due to the crystallization of η-Al_2O_3 and to the phase transformation from η-Al_2O_3 to α-Al_2O_3, respectively (Fig. 6). At 1100 °C, weak peaks corresponding to Mn_3O_4 [23] were also observed, which reacted at higher temperatures (1400 °C) with the aluminum oxide to form a spinel with composition $MnAl_2O_4$ coexisting with an excess of α-Al_2O_3 (Fig. 6). It should be noted that after heating at 1100 °C, the particles were still spherical, showing a shrinkage with respect to the as-prepared powder similar to that observed for sample 12.5Cr (Fig. 1B). The spherical shape was lost at 1400 °C as a consequence of particle sintering (Fig. 7A).

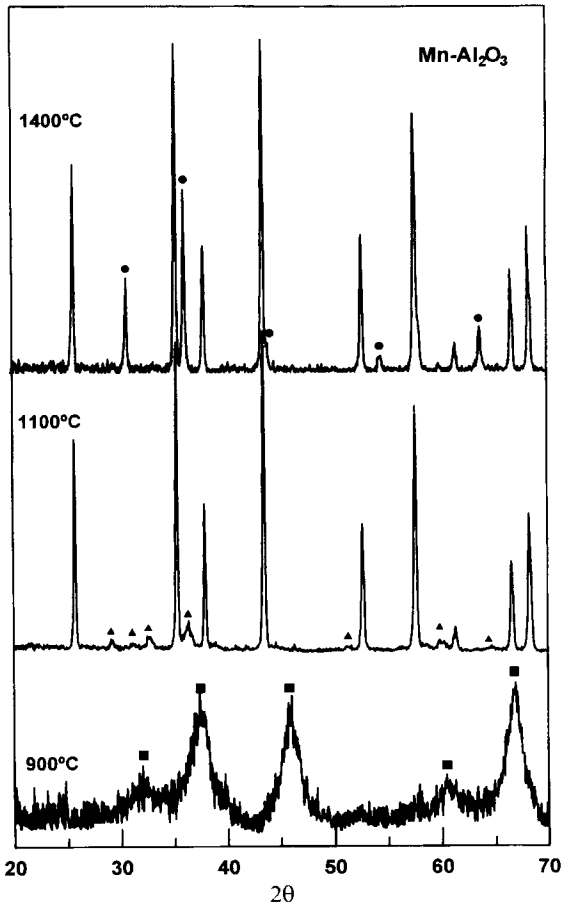

Fig. 6 X-ray diffraction patterns obtained for sample 10.8Mn after heating at different temperatures. Symbols designating different phases: (■) η-Al_2O_3, (▲) Mn_3O_4 and (●) $MnAl_2O_4$. Unlabelled peaks correspond to α-Al_2O_3

The structural evolution of the other prepared Mn-doped alumina samples (Table 1) with temperature was similar to that described above, except that the complete formation of the spinel phase took place at higher temperature (1500 °C).

Since Mn-doped alumina is considered as a corundum-type pigment [11], the color of the Mn-doped alumina samples was evaluated after corundum crystallization (1100–1400 °C). The $L^*a^*b^*$ parameters of sample 10.8Mn heated at 1100 °C corresponded to a strong brown color, which remained unaltered with increasing temperature up to 1400 °C (Table 3), in spite of the change in the nature of the chromophore agent from Mn_3O_4 (1100 °C) to $MnAl_2O_4$ (1400 °C) (Fig. 6). The same color properties ($L^*a^*b^*$ values) were observed when the Mn/Al mole ratio was reduced from 10.8% to 8.7%, keeping the same calcination conditions (Table 3). This finding seems to indicate that a certain degree of color saturation was attained

Colloid & Polymer Science, Vol. 275, No. 11 (1997)

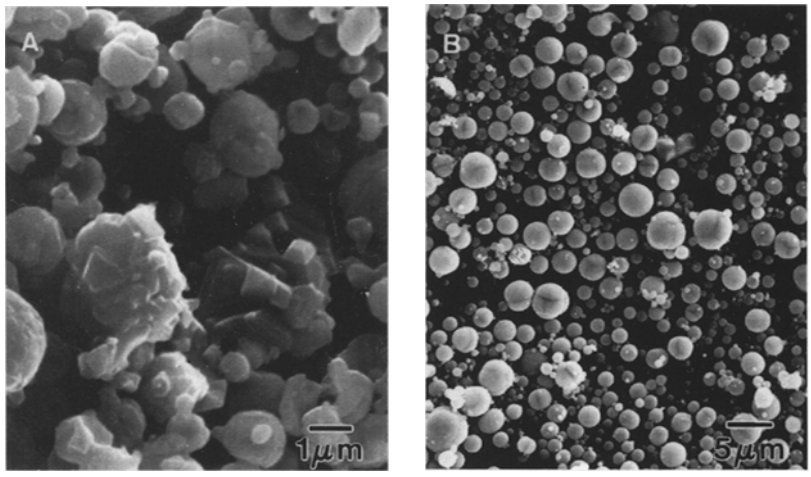

Fig. 7 SEM micrographs of: (A) sample 10.8Mn heated at 1400 °C; and (B) sample 10.7Co heated at 1300 °C

for a Mn/Al ratio of about 8.7%. A further decrease in the Mn content to 2.8% gave rise to a progressive increase of the L^* value (Table 3), i.e., to a decrease of the color intensity.

The electrophoretic mobilities of sample 10.8Mn heated at 1100 °C (Fig. 5) gave an i.e.p. higher (6.1) than that corresponding to the blank (5.2) indicating that Mn_3O_4 may be preferentially located at the particle outer layers.

Co-doped alumina

Table 1 shows the Co/Al mole ratio of the as-prepared Co-doped alumina samples. As expected, no significant differences in the morphological features, composition and structure were detected in these powders with respect to those doped with Cr or Mn, except the change in the nature of the doping cation.

The DTA curve of sample 10.7Co was also very similar to that of sample 12.5Cr (Fig. 3) showing an endothermic peak at 105 °C due to the release of water, and several exothermic ones between 200 and 350 °C attributed to the decomposition of organic impurities and nitrate anions. Finally, only one exothermic effect was observed at higher temperature (815 °C), the origin of which will be discussed further.

The X-ray diffraction patterns of sample 10.7Co heated at different temperatures are presented in Fig. 8. No crystalline phases were detected at <700 °C. Although at this temperature some material still remains amorphous, as revealed by the broad feature at 2θ–$20°$, several weak peaks appeared that could be attributed to either Co_3O_4 or $CoAl_2O_4$, since their X-ray diffraction patterns are very similar [24, 25]. On the basis of the phase diagram of the

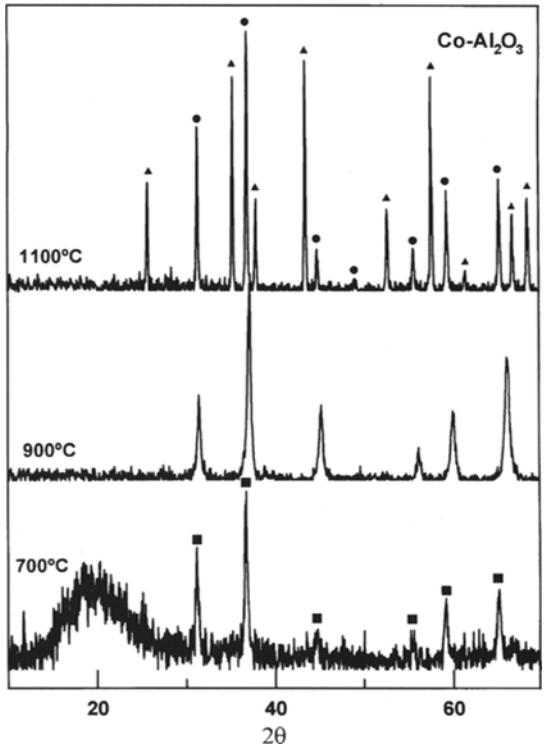

Fig. 8 X-ray diffraction patterns obtained for sample 10.7Co after heating at different temperatures. Symbols designating different phases: (■) Co_3O_4, (▲) α-Al_2O_3 and (●) $CoAl_2O_4$. Unlabelled peaks are slightly shifted with respect to those of $CoAl_2O_4$

CoO–Al_2O_3 system [26] which shows the formation of the $CoAl_2O_4$ spinel at >1000 °C, we think that in this case, the crystalline phase must probably consist of Co_3O_4. The calcination of the sample at 900 °C gave rise to a shift of the position of the Co_3O_4 peaks to higher

2θ values, and therefore to a decrease of the interplanar spacings value. Such a behavior could be interpreted if we assume the diffusion of some Al^{3+} cations towards the tetrahedral positions of Co^{2+} in the Co_3O_4 lattice, which would produce a cell compression since the ionic radius of the later (0.72 Å) [27] is higher than that of the aluminum cation (0.5 Å) [27]. Notice that the incorporation of Al^{3+} only to the octahedral positions of Co^{3+} (ionic radius = 0.63 Å) [27] would lead to the formation of the normal $CoAl_2O_4$ spinel which did not show appreciable differences in the cell dimensions with respect to Co_3O_4 [24, 25]. Such a diffusion process could be responsible for the exothermic effect detected at 815 °C by DTA (Fig. 3). The appropriate atoms arrangement to form the normal $CoAl_2O_4$ spinel required a heat treatment at 1100 °C, at which temperature, the crystallization of α-Al_2O_3 also took place (Fig. 8). Under these conditions, the particles were still spherical and showed a size distribution similar to that of sample 12.5Cr heated at 500 °C (Fig. 1B). No further morphological (Fig. 7B) or structural changes were observed on calcination at higher temperatures up to 1300 °C.

The $L^*a^*b^*$ parameters of the Co-doped alumina samples heated at different temperatures above that of the Co–Al spinel formation ($\geq$1100 °C) are included in Table 3. Sample 10.7Co heated at 1100 °C showed the bright blue color characteristic of $CoAl_2O_4$, whose properties (hue and intensity) were not modified by increasing the temperature up to 1300 °C. Finally, as the Co/Al ratio was reduced from 10.7% to 2.8%, an increase of L^* and a decrease of b^* were observed (Table 3), indicating a decrease in the blue color intensity.

The i.e.p. obtained from the electrophoretic mobilities of sample 10.7Co heated at 1100 °C, was 5.9 (Fig. 5). This increase with respect to the i.e.p. of the blank (5.2) seems to indicate the presence of the $CoAl_2O_4$ spinel at the particles outer layers.

Acknowledgements This work was supported by the Spanish DGCYT under Project PB95-0225. The help of Dr. P. Tartaj in measuring i.e.p. is gratefully acknowledged.

References

1. Classification and chemical description of the complex inorganic color pigments (1991) In: Dry Color Manufacturer's Association. Alexandria, VA, pp 10, 233
2. Matijević E (1986) Langmuir 2:12
3. Ocaña M, Serna CJ (1996) Mat Tech 10:151
4. Visca M, Matijević E (1979) J Colloid Interface Sci 68:308
5. Ingebrethsen B, Matijević E (1980) J Aerosol Sci 11:271
6. Ocaña M, Matijević E (1990) J Aerosol Sci 21:811
7. Ocaña M, Fornés V, Serna CJ (1992) Ceram Int 18:99
8. Balboa A, Parch RE, Matijević E (1987) Colloids Surfaces 27:123
9. Ocaña M, Sanz J, González-Carreño T, Serna CJ (1993) J Am Ceram Soc 76:2081
10. Mayville FC, Partch RE, Matijević E (1987) J Colloid Interface Sci 120:135
11. Ocaña M, Levy D, Serna CJ (1992) J Non-Cryst Solids 147, 148:621
12. Ingebrethsen B, Matijević E (1984) J Colloid Interface Sci 100:1
13. Tartaj P, Serna CJ, Ocaña M (1995) J Am Ceram Soc 78:1147
14. ASTM card No 10-173
15. Natl Bur Stad (US) Monogr (1976) 25:1335
16. C.I.E. Publ. No 15 (E1-1.31) 1971 (1978) Bureau Central de la C.I.E., Paris
17. Nakamoto K (1986) Infrared and Raman Spectra of Inorganic and Coordination Compounds. Wiley, New York, pp 476
18. ASTM card No 29-63
19. ASTM card No 4-875
20. Wefers K, Misra C (1987) Oxides and Hydroxides of Aluminum, Alcoa Technical Paper No 19, Revised, Alcoa Laboratories, Pittsburg, PA
21. Tcheichvili L, Weyl WA (1963) Glass Industry 44:208
22. Parks GA (1965) Chem Rev 65:177
23. ASTM card No 24-734
24. ASTM card No 9-418
25. ASTM card No 10-458
26. Mori T (1982) Yogyo Kyokaishi 90:100
27. Lide DR (ed) (1992) Handbook of Chemistry and Physics. CRC Press, Boston, pp 12-8